Cavendish-HEP-03/16
LBNL-53599

Next-to-next-to-leading order soft-gluon corrections in top quark hadroproduction

Nikolaos Kidonakis[a] and Ramona Vogt[b]

[a] *Cavendish Laboratory, University of Cambridge, Madingley Road, Cambridge CB3 0HE, UK*

[b] *Nuclear Science Division, Lawrence Berkeley National Laboratory, Berkeley, CA 94720, USA and Physics Department, University of California at Davis, Davis, CA 95616, USA*

Abstract

We calculate next-to-next-to-leading order soft-gluon corrections to top quark total and differential cross sections in hadron colliders. We increase the accuracy of our previous estimates by including additional subleading terms, including next-to-next-to-next-to-leading-logarithmic and some virtual terms. We show that the kinematics dependence of the cross section vanishes near threshold and is reduced away from it. The factorization and renormalization scale dependence of the cross section is also greatly reduced. We present results for the top quark total cross sections and transverse momentum distributions at the Tevatron and the LHC.

1 Introduction

The discovery of the top quark in $p\bar{p}$ collisions at Run I of the Tevatron in 1995 [1] and its observation currently at Run II, with expected increases in the accuracy of the top mass and cross section measurements, have made theoretical calculations of top production cross sections and differential distributions an interesting and topical subject. The latest calculation for top hadroproduction includes next-to-next-to-leading-order (NNLO) soft-gluon corrections to the double differential cross section [2, 3] from threshold resummation techniques [4, 5, 6]. Near threshold there is limited phase space for the emission of real gluons so that soft-gluon corrections dominate the cross section.

These soft corrections take the form of logarithms, $[\ln^l(x_{\rm th})/x_{\rm th}]_+$, with $l \leq 2n-1$ for the order α_s^n corrections, where $x_{\rm th}$ is a kinematical variable that measures distance from threshold and goes to zero at threshold. NNLO calculations for top quark production have so far been done through next-to-next-to-leading-logarithmic (NNLL) accuracy, i.e. including leading logarithms (LL) with $l = 3$, next-to-leading logarithms (NLL) with $l = 2$, and NNLL with $l = 1$, at NNLO [2, 3]. This NNLO-NNLL calculation has had great success in significantly reducing the factorization/renormalization scale dependence of the cross section. Indeed the scale dependence of top production is almost negligible. However, the dependence of the corrections on the kinematics choice is substantial. In Ref. [3], the top cross section was studied in both single-particle-inclusive (1PI) and pair-invariant-mass (PIM) kinematics. Important differences between the two kinematics choices were found in both the parton-level and hadron-level cross sections, even near threshold. Similar kinematics effects were found for bottom and charm hadroproduction [3, 7]. Thus subleading, beyond NNLL, contributions can still have an impact on the cross section. If all the NNLO soft corrections are included, there should be no difference between the two kinematics near threshold. If all NNLO corrections, both soft and hard, were known, there should be no difference between the two kinematics, even far from threshold. Away from threshold, where the approximations of Ref. [3] are not expected to apply since real emission of hard gluons comes into play, the discrepancy between the 1PI and PIM results is not surprising. However, the NNLO-NNLL calculation exhibits some notable discrepancies between the two kinematics even at the lowest η, where $\eta = s/(4m^2) - 1 \to 0$ at threshold. Thus, additional subleading terms are clearly needed to bring the calculation under further theoretical control.

In this paper, we include additional subleading NNLO soft corrections, including next-to-next-to-next-to-leading logarithms (NNNLL) with $l = 0$, as well as some virtual $\delta(x_{\rm th})$ corrections. We apply the method and results of Ref. [8], based on earlier resummation studies [4, 5, 6], where master formulas are given for the NNLO soft and virtual corrections for processes in hadron-hadron and lepton-hadron collisions. As we will see, the subleading corrections do indeed bring the 1PI and PIM results into agreement near threshold for both the $q\overline{q} \to t\overline{t}$ and the $gg \to t\overline{t}$ channels, while the discrepancies away from threshold are also diminished, especially in the gg channel. Thus the threshold region is brought under theoretical control.

Since the resummation formalism has been reviewed extensively in Refs. [2, 3, 4, 5, 8], we only provide a rough outline here. Threshold resummation is a method of formally calculating contributions from soft-gluon emission to all orders in perturbation theory. The resummation is normally carried out in moment space where N is the variable conjugate to $x_{\rm th}$ and the leading threshold logarithms are of the form $\ln^{2n} N$ for the order α_s^n corrections. The resummed cross section, in moment space, can then be expanded to NNLO (and even higher orders [2]) and

the finite-order result finally inverted back to momentum space. The previous calculations of Refs. [2, 3] and the universal results of Ref. [8] employ this approach.

In the following section we give the analytical form of the NNLO soft and (some) virtual corrections in the $q\overline{q} \to t\overline{t}$ channel in both 1PI and PIM kinematics. In Section 3 we give the results for the $gg \to t\overline{t}$ channel. Note that while we refer only to $t\overline{t}$ here, the results in Sections 2 and 3 are equally valid for all heavy quarks. Section 4 discusses the partonic cross sections in both channels. In Section 5 we present the hadronic cross sections and transverse momentum distributions for top production in Tevatron Run I and Run II as well as at the LHC. We conclude with a summary in Section 6.

2 NNLO soft corrections to $q\overline{q} \to t\overline{t}$

We first study the $q\overline{q} \to t\overline{t}$ process. Before discussing the corrections, we introduce our kinematics notation (the same notation will also be used for $gg \to t\overline{t}$). In 1PI kinematics the process is

$$q(p_a) + \overline{q}(p_b) \longrightarrow t(p_1) + X[\overline{t}](p_2) \tag{2.1}$$

where t is an identified top quark of mass m and $X[\overline{t}]$ is the remaining final state that contains the $\overline{t}$. We define the kinematical invariants $s = (p_a+p_b)^2$, $t_1 = (p_b-p_1)^2-m^2$, $u_1 = (p_a-p_1)^2-m^2$ and $s_4 = s+t_1+u_1$. At threshold, $s_4 \to 0$, and the soft corrections appear as $[\ln^l(s_4/m^2)/s_4]_+$.

In PIM kinematics, we have instead

$$q(p_a) + \overline{q}(p_b) \longrightarrow t\overline{t}(p) + X(k)\,. \tag{2.2}$$

At partonic threshold, $s = M^2$, M^2 is the pair mass squared, and $t_1 = -(M^2/2)(1-\beta_M \cos\theta)$, $u_1 = -(M^2/2)(1+\beta_M \cos\theta)$ where $\beta_M = \sqrt{1-4m^2/M^2}$ and θ is the scattering angle in the parton center-of-mass frame. The soft corrections appear as $[\ln^l(1-z)/(1-z)]_+$ with $z = M^2/s \to 1$ at threshold.

A more detailed discussion of the kinematics can be found in Ref. [3].

2.1 $q\overline{q} \to t\overline{t}$ channel in 1PI kinematics

We begin our study with the next-to-leading order (NLO) corrections. In the $\overline{\rm MS}$ scheme, the NLO soft and virtual corrections for $q\overline{q} \to t\overline{t}$ in 1PI kinematics can be written as

$$s^2\,\frac{d^2\hat{\sigma}^{(1)\ 1\rm PI}_{q\overline{q}}}{dt_1\,du_1} = F^{B\ 1\rm PI}_{q\overline{q}}\frac{\alpha_s(\mu_R^2)}{\pi}\left\{c^{1\rm PI}_{3\ q\overline{q}}\left[\frac{\ln(s_4/m^2)}{s_4}\right]_+ + c^{1\rm PI}_{2\ q\overline{q}}\left[\frac{1}{s_4}\right]_+ + c^{1\rm PI}_{1\ q\overline{q}}\,\delta(s_4)\right\}. \tag{2.3}$$

Here, the Born term is

$$F^{B\ 1\rm PI}_{q\overline{q}} = \pi\alpha_s^2(\mu_R^2)K_{q\overline{q}}N_cC_F\left[\frac{t_1^2+u_1^2}{s^2}+\frac{2m^2}{s}\right] \tag{2.4}$$

where μ_R is the renormalization scale, $C_F = (N_c^2-1)/(2N_c)$ with $N_c = 3$ the number of colors, and $K_{q\overline{q}} = N_c^{-2}$ is a color average factor.

We also have $c_{3\,q\overline{q}}^{\rm 1PI} = 4C_F$ and

$$\begin{aligned} c_{2\,q\overline{q}}^{\rm 1PI} &= 2C_F\left[4\ln\left(\frac{u_1}{t_1}\right) - \ln\left(\frac{t_1u_1}{m^4}\right) - L'_\beta - 1 - \ln\left(\frac{\mu_F^2}{s}\right)\right] \\ &\quad + C_A\left[-3\ln\left(\frac{u_1}{t_1}\right) - \ln\left(\frac{m^2 s}{t_1u_1}\right) + L'_\beta\right], \end{aligned} \tag{2.5}$$

where μ_F is the factorization scale, $C_A = N_c$, $L'_\beta = [(1-2m^2/s)/\beta]\ln[(1-\beta)/(1+\beta)]$ and $\beta = \sqrt{1-4m^2/s}$. For later use, we write

$$c_{2\,q\overline{q}}^{\rm 1PI} \equiv T_{2\,q\overline{q}}^{\rm 1PI} - 2C_F\ln\left(\frac{\mu_F^2}{s}\right), \tag{2.6}$$

so that $T_{2\,q\overline{q}}^{\rm 1PI}$ is the scale-independent part of $c_{2\,q\overline{q}}^{\rm 1PI}$. Finally,

$$c_{1\,q\overline{q}}^{\rm 1PI} = \frac{\sigma_{q\overline{q}\,\delta}^{(1)\,S+V\;1{\rm PI}}}{(\alpha_s/\pi)F_{q\overline{q}}^{B\;1{\rm PI}}} \tag{2.7}$$

where $\sigma_{q\overline{q}\,\delta}^{(1)\,S+V\;1{\rm PI}}$ denotes the $\delta(s_4)$ terms in Eq. (4.7) of Ref. [9] with the definitions of t_1 and u_1 interchanged with respect to that reference. We also write

$$c_{1\,q\overline{q}}^{\rm 1PI} \equiv T_{1\,q\overline{q}}^{\rm 1PI} + C_F\left[-\frac{3}{2} + \ln\left(\frac{t_1u_1}{m^4}\right)\right]\ln\left(\frac{\mu_F^2}{s}\right) + \frac{\beta_0}{2}\ln\left(\frac{\mu_R^2}{s}\right), \tag{2.8}$$

where $T_{1\,q\overline{q}}^{\rm 1PI}$ has no scale dependence.

Before presenting the NNLO soft corrections, we define the constants $\zeta_2 = \pi^2/6$, $\zeta_4 = \pi^4/90$, and $\zeta_3 = 1.2020569\cdots$, and the two-loop constant $K = C_A(67/18 - \pi^2/6) - 5n_f/9$, with n_f the number of light quark flavors. Finally, we define

$$\beta(\alpha_s) \equiv \mu\,\frac{d\ln g}{d\mu} = -\beta_0\frac{\alpha_s}{4\pi} - \beta_1\frac{\alpha_s^2}{(4\pi)^2} + \cdots, \tag{2.9}$$

where $\beta_0 = (11C_A - 2n_f)/3$ and

$$\beta_1 = \frac{34}{3}C_A^2 - 2n_f\left(C_F + \frac{5}{3}C_A\right). \tag{2.10}$$

Following Ref. [8] we write the NNLO soft-plus-virtual corrections in 1PI kinematics as

$$\begin{aligned} s^2\,\frac{d^2\hat{\sigma}_{q\overline{q}}^{(2)\;1{\rm PI}}}{dt_1\,du_1} &= F_{q\overline{q}}^{B\;1{\rm PI}}\frac{\alpha_s^2(\mu_R^2)}{\pi^2}\left\{\frac{1}{2}\left(c_{3\,q\overline{q}}^{\rm 1PI}\right)^2\left[\frac{\ln^3(s_4/m^2)}{s_4}\right]_+ + \left[\frac{3}{2}c_{3\,q\overline{q}}^{\rm 1PI}\,c_{2\,q\overline{q}}^{\rm 1PI} - \frac{\beta_0}{4}c_{3\,q\overline{q}}^{\rm 1PI}\right]\left[\frac{\ln^2(s_4/m^2)}{s_4}\right]_+\right. \\ &\quad + \left[c_{3\,q\overline{q}}^{\rm 1PI}\,c_{1\,q\overline{q}}^{\rm 1PI} + \left(c_{2\,q\overline{q}}^{\rm 1PI}\right)^2 - \zeta_2\left(c_{3\,q\overline{q}}^{\rm 1PI}\right)^2 - \frac{\beta_0}{2}T_{2\,q\overline{q}}^{\rm 1PI} + \frac{\beta_0}{4}c_{3\,q\overline{q}}^{\rm 1PI}\ln\left(\frac{\mu_R^2}{s}\right)\right. \\ &\qquad \left.+ 2C_FK + 8\frac{C_F}{C_A}\ln^2\left(\frac{u_1}{t_1}\right)\right]\left[\frac{\ln(s_4/m^2)}{s_4}\right]_+ \\ &\quad + \left[c_{2\,q\overline{q}}^{\rm 1PI}\,c_{1\,q\overline{q}}^{\rm 1PI} - \zeta_2\,c_{2\,q\overline{q}}^{\rm 1PI}\,c_{3\,q\overline{q}}^{\rm 1PI} + \zeta_3\left(c_{3\,q\overline{q}}^{\rm 1PI}\right)^2 - \frac{\beta_0}{2}T_{1\,q\overline{q}}^{\rm 1PI} + \frac{\beta_0}{4}c_{2\,q\overline{q}}^{\rm 1PI}\ln\left(\frac{\mu_R^2}{s}\right) + \mathcal{G}_{q\overline{q}}^{(2)}\right. \\ &\qquad \left.+ C_F\frac{\beta_0}{4}\ln^2\left(\frac{\mu_F^2}{s}\right) - C_FK\ln\left(\frac{\mu_F^2}{s}\right) - C_FK\ln\left(\frac{t_1u_1}{m^4}\right) + 8\frac{C_F}{C_A}\ln^2\left(\frac{u_1}{t_1}\right)\ln\left(\frac{m^2}{s}\right)\right]\left[\frac{1}{s_4}\right]_+ \\ &\quad \left. + R_{q\overline{q}}^{\rm 1PI}\delta(s_4)\right\}. \end{aligned} \tag{2.11}$$

Here

$$\mathcal{G}^{(2)}_{q\overline{q}} = C_F C_A \left(\frac{7}{2}\zeta_3 + \frac{22}{3}\zeta_2 - \frac{299}{27}\right) + n_f C_F \left(-\frac{4}{3}\zeta_2 + \frac{50}{27}\right) \tag{2.12}$$

denotes a set of two-loop contributions that are universal for processes with $q\overline{q}$ initial states [8]. Process-dependent two-loop corrections [10] are not included in $\mathcal{G}^{(2)}_{q\overline{q}}$ but, as we will see in Section 4, their contribution is expected to be negligible. The virtual contribution $R^{\rm 1PI}_{q\overline{q}}$ is not fully known. However, we can determine certain terms in $R^{\rm 1PI}_{q\overline{q}}$ exactly. These exact terms involve the factorization and renormalization scales as well as the those terms that arise from the inversion from moment to momentum space (for a detailed discussion of the inversion procedure see Section IIIC and Appendix A of Ref. [2]).

The terms multiplying $\delta(s_4)$ involving the factorization and renormalization scales are given explicitly by

$$\begin{aligned}
F^{B\,\rm 1PI}_{q\overline{q}} \frac{\alpha_s^2(\mu_R^2)}{\pi^2} \Bigg[& \ln^2\left(\frac{\mu_F^2}{m^2}\right) \left\{ \frac{C_F^2}{2} \left[\ln\left(\frac{t_1\,u_1}{m^4}\right) - \frac{3}{2}\right]^2 - 2\zeta_2 C_F^2 + \frac{\beta_0}{8} C_F \left[\frac{3}{2} - \ln\left(\frac{t_1\,u_1}{m^4}\right)\right] \right\} \\
& + \ln\left(\frac{\mu_F^2}{m^2}\right) \ln\left(\frac{\mu_R^2}{m^2}\right) \frac{3\beta_0}{4} C_F \left[\ln\left(\frac{t_1\,u_1}{m^4}\right) - \frac{3}{2}\right] + \ln^2\left(\frac{\mu_R^2}{m^2}\right) \frac{3\beta_0^2}{16} \\
& + \ln\left(\frac{\mu_F^2}{m^2}\right) \left\{ C_F^2 \left[\ln\left(\frac{t_1\,u_1}{m^4}\right) - \frac{3}{2}\right]^2 \ln\left(\frac{m^2}{s}\right) + C_F \left[\ln\left(\frac{t_1\,u_1}{m^4}\right) - \frac{3}{2}\right] \left[T^{\rm 1PI}_{1\,q\overline{q}} + \frac{\beta_0}{2} \ln\left(\frac{m^2}{s}\right)\right] \right. \\
& \qquad \left. + 2C_F\zeta_2 \left[T^{\rm 1PI}_{2\,q\overline{q}} - 2C_F \ln\left(\frac{m^2}{s}\right)\right] - 8C_F^2\zeta_3 + C_F \frac{K}{2} \ln\left(\frac{t_1\,u_1}{m^4}\right) - 2\gamma'^{(2)}_{q/q} \right\} \\
& + \ln\left(\frac{\mu_R^2}{m^2}\right) \left\{ \frac{3\beta_0}{4} \left[C_F \left(\ln\left(\frac{t_1\,u_1}{m^4}\right) - \frac{3}{2}\right) \ln\left(\frac{m^2}{s}\right) + \frac{\beta_0}{2} \ln\left(\frac{m^2}{s}\right) + T^{\rm 1PI}_{1\,q\overline{q}} \right] + \frac{\beta_1}{8} \right\} \Bigg]
\end{aligned} \tag{2.13}$$

where

$$\gamma'^{(2)}_{q/q} = C_F^2 \left(\frac{3}{32} - \frac{3}{4}\zeta_2 + \frac{3}{2}\zeta_3\right) + C_F C_A \left(-\frac{3}{4}\zeta_3 + \frac{11}{12}\zeta_2 + \frac{17}{96}\right) + n_f C_F \left(-\frac{\zeta_2}{6} - \frac{1}{48}\right). \tag{2.14}$$

The terms multiplying $\delta(s_4)$ resulting from inversion (ζ terms) that do not involve the factorization and renormalization scales are [2, 8]

$$\begin{aligned}
F^{B\,\rm 1PI}_{q\overline{q}} \frac{\alpha_s^2(\mu_R^2)}{\pi^2} \Bigg\{ & -\frac{\zeta_2}{2} \left[T^{\rm 1PI}_{2\,q\overline{q}} - 2C_F \ln\left(\frac{m^2}{s}\right)\right]^2 + \frac{1}{4}\zeta_2^2 \left(c^{\rm 1PI}_{3\,q\overline{q}}\right)^2 + \zeta_3\, c^{\rm 1PI}_{3\,q\overline{q}} \left[T^{\rm 1PI}_{2\,q\overline{q}} - 2C_F \ln\left(\frac{m^2}{s}\right)\right] \\
& - \frac{3}{4}\zeta_4 \left(c^{\rm 1PI}_{3\,q\overline{q}}\right)^2 - 4\zeta_2 \frac{C_F}{C_A} \ln^2\left(\frac{u_1}{t_1}\right) \Bigg\}.
\end{aligned} \tag{2.15}$$

2.2 $q\overline{q} \to t\overline{t}$ channel in PIM kinematics

Next, we study the soft-gluon corrections in PIM kinematics. The $\overline{\rm MS}$ NLO soft and virtual corrections to $q\overline{q} \to t\overline{t}$ in PIM kinematics are

$$s\,\frac{d^2\hat{\sigma}^{(1)\,\rm PIM}_{q\overline{q}}}{dM^2\,d\cos\theta} = F^{B\,\rm PIM}_{q\overline{q}} \frac{\alpha_s(\mu_R^2)}{\pi} \left\{ c^{\rm PIM}_{3\,q\overline{q}} \left[\frac{\ln(1-z)}{1-z}\right]_+ + c^{\rm PIM}_{2\,q\overline{q}} \left[\frac{1}{1-z}\right]_+ + c^{\rm PIM}_{1\,q\overline{q}} \delta(1-z) \right\}. \tag{2.16}$$

Here the Born term is

$$F^{B\,\rm PIM}_{q\overline{q}} = \frac{\beta}{2s} F^{B\,\rm 1PI}_{q\overline{q}}|_{\rm PIM} = \frac{\beta}{2s} \pi\alpha_s^2 K_{q\overline{q}} N_c C_F \left[\frac{1}{2}\left(1 + \beta^2\cos^2\theta\right) + \frac{2m^2}{s}\right], \tag{2.17}$$

where $|_{\rm PIM}$ indicates that for t_1, u_1 we use the expressions below Eq. (2.2). Also $c_{3\,q\overline{q}}^{\rm PIM} = 4C_F$,

$$\begin{aligned} c_{2\,q\overline{q}}^{\rm PIM} &= 2C_F\left[4\ln\left(\frac{u_1}{t_1}\right) - L'_\beta - 1 - \ln\left(\frac{\mu_F^2}{s}\right)\right] \\ &\quad + C_A\left[-3\ln\left(\frac{u_1}{t_1}\right) - \ln\left(\frac{m^2 s}{t_1 u_1}\right) + L'_\beta\right], \\ &\equiv T_{2\,q\overline{q}}^{\rm PIM} - 2C_F\ln\left(\frac{\mu_F^2}{s}\right), \end{aligned} \tag{2.18}$$

and

$$c_{1\,q\overline{q}}^{\rm PIM} \equiv T_{1\,q\overline{q}}^{\rm PIM} - \frac{3}{2}C_F\ln\left(\frac{\mu_F^2}{s}\right) + \frac{\beta_0}{2}\ln\left(\frac{\mu_R^2}{s}\right). \tag{2.19}$$

Note that the scale-independent $T_{1\,q\overline{q}}^{\rm PIM}$ is related to its 1PI counterpart by

$$T_{1\,q\overline{q}}^{\rm PIM} = 2T_{1\,q\overline{q}}^{\rm 1PI}|_{\rm PIM} + \frac{1}{F_{q\overline{q}}^{B\,\rm PIM}}\, s\,\frac{d^2\sigma'^{(1)\,\rm S+MF}_{q\overline{q}}}{dM^2\,d\cos\theta} - \frac{1}{F_{q\overline{q}}^{B\,\rm PIM}}\,\frac{\beta}{s}\,s^2\,\frac{d^2\sigma'^{(1)\,\rm S+MF}_{q\overline{q}}}{dt_1\,du_1}|_{\rm PIM}. \tag{2.20}$$

Here $\sigma'^{(1)\,\rm S+MF}_{q\overline{q}}$ denotes the soft and mass factorization subtraction terms calculated in Ref. [3]. The prime indicates that we drop the overall $\delta(1-z)$ or $\delta(s_4)$ coefficient from the expressions in Eqs. (82), (A8), and (A9) of Ref. [3].

In PIM kinematics, the NNLO soft-plus-virtual corrections are

$$\begin{aligned} s\,\frac{d^2\hat{\sigma}^{(2)\,\rm PIM}_{q\overline{q}}}{dM^2\,d\cos\theta} &= F_{q\overline{q}}^{B\,\rm PIM}\frac{\alpha_s^2(\mu_R^2)}{\pi^2}\left\{\frac{1}{2}\left(c_{3\,q\overline{q}}^{\rm PIM}\right)^2\left[\frac{\ln^3(1-z)}{1-z}\right]_+ + \left[\frac{3}{2}c_{3\,q\overline{q}}^{\rm PIM}\,c_{2\,q\overline{q}}^{\rm PIM} - \frac{\beta_0}{4}c_{3\,q\overline{q}}^{\rm PIM}\right]\left[\frac{\ln^2(1-z)}{1-z}\right]_+\right. \\ &\quad + \left[c_{3\,q\overline{q}}^{\rm PIM}\,c_{1\,q\overline{q}}^{\rm PIM} + \left(c_{2\,q\overline{q}}^{\rm PIM}\right)^2 - \zeta_2\left(c_{3\,q\overline{q}}^{\rm PIM}\right)^2 - \frac{\beta_0}{2}T_{2\,q\overline{q}}^{\rm PIM} + \frac{\beta_0}{4}c_{3\,q\overline{q}}^{\rm PIM}\ln\left(\frac{\mu_R^2}{s}\right)\right. \\ &\qquad \left.+ 2C_F K + 8\frac{C_F}{C_A}\ln^2\left(\frac{u_1}{t_1}\right)\right]\left[\frac{\ln(1-z)}{1-z}\right]_+ \\ &\quad + \left[c_{2\,q\overline{q}}^{\rm PIM}\,c_{1\,q\overline{q}}^{\rm PIM} - \zeta_2\,c_{2\,q\overline{q}}^{\rm PIM}\,c_{3\,q\overline{q}}^{\rm PIM} + \zeta_3\left(c_{3\,q\overline{q}}^{\rm PIM}\right)^2 - \frac{\beta_0}{2}T_{1\,q\overline{q}}^{\rm PIM} + \frac{\beta_0}{4}c_{2\,q\overline{q}}^{\rm PIM}\ln\left(\frac{\mu_R^2}{s}\right) + \mathcal{G}_{q\overline{q}}^{(2)}\right. \\ &\qquad \left.+ C_F\frac{\beta_0}{4}\ln^2\left(\frac{\mu_F^2}{s}\right) - C_F K\ln\left(\frac{\mu_F^2}{s}\right)\right]\left[\frac{1}{1-z}\right]_+ \\ &\quad \left.+ R_{q\overline{q}}^{\rm PIM}\delta(1-z)\right\}. \end{aligned} \tag{2.21}$$

Again, only certain terms in $R_{q\overline{q}}^{\rm PIM}$ that can be determined exactly are included. The terms multiplying $\delta(1-z)$ that involve the factorization and renormalization scales are

$$\begin{aligned} &F_{q\overline{q}}^{B\,\rm PIM}\frac{\alpha_s^2(\mu_R^2)}{\pi^2}\left[\ln^2\left(\frac{\mu_F^2}{m^2}\right)\left\{\frac{9}{8}C_F^2 - 2\zeta_2 C_F^2 + \frac{3}{16}C_F\beta_0\right\}\right. \\ &\qquad - \frac{9}{8}\beta_0\,C_F\ln\left(\frac{\mu_F^2}{m^2}\right)\ln\left(\frac{\mu_R^2}{m^2}\right) + \frac{3\beta_0^2}{16}\ln^2\left(\frac{\mu_R^2}{m^2}\right) \\ &\qquad \left. + \ln\left(\frac{\mu_F^2}{m^2}\right)\left\{\frac{9}{4}C_F^2\ln\left(\frac{m^2}{s}\right) - \frac{3}{2}C_F\left[T_{1\,q\overline{q}}^{\rm PIM} + \frac{\beta_0}{2}\ln\left(\frac{m^2}{s}\right)\right]\right. \end{aligned}$$

$$+ 2C_F\zeta_2\left[T_{2\,q\overline{q}}^{\rm PIM} - 2C_F\ln\left(\frac{m^2}{s}\right)\right] - 8C_F^2\zeta_3 - 2\gamma'^{(2)}_{q/q}\Bigg\}$$
$$+ \ln\left(\frac{\mu_R^2}{m^2}\right)\left\{\frac{3\beta_0}{4}\left[-\frac{3}{2}C_F\ln\left(\frac{m^2}{s}\right) + \frac{\beta_0}{2}\ln\left(\frac{m^2}{s}\right) + T_{1\,q\overline{q}}^{\rm PIM}\right] + \frac{\beta_1}{8}\right\}\Bigg] . \qquad (2.22)$$

The terms multiplying $\delta(1-z)$ that arise from inversion and do not involve the factorization and renormalization scales are given by

$$F_{q\overline{q}}^{B\,\rm PIM}\frac{\alpha_s^2(\mu_R^2)}{\pi^2}\left\{-\frac{\zeta_2}{2}\left[T_{2\,q\overline{q}}^{\rm PIM} - 2C_F\ln\left(\frac{m^2}{s}\right)\right]^2 + \frac{1}{4}\zeta_2^2\left(c_{3\,q\overline{q}}^{\rm PIM}\right)^2\right.$$
$$\left. + \zeta_3\, c_{3\,q\overline{q}}^{\rm PIM}\left[T_{2\,q\overline{q}}^{\rm PIM} - 2C_F\ln\left(\frac{m^2}{s}\right)\right] - \frac{3}{4}\zeta_4\left(c_{3\,q\overline{q}}^{\rm PIM}\right)^2 - 4\zeta_2\frac{C_F}{C_A}\ln^2\left(\frac{u_1}{t_1}\right)\right\} . \qquad (2.23)$$

3 NNLO soft corrections to $gg \to t\bar{t}$

3.1 $gg \to t\bar{t}$ channel in 1PI kinematics

We now turn to the gg channel. We write the $\overline{\rm MS}$ NLO soft-plus-virtual corrections for $gg \to t\bar{t}$ in 1PI kinematics as

$$s^2\,\frac{d^2\hat{\sigma}_{gg}^{(1)\,\rm 1PI}}{dt_1\,du_1} = F_{gg}^{B\,\rm 1PI}\frac{\alpha_s(\mu_R^2)}{\pi}\left\{c_{3\,gg}^{\rm 1PI}\left[\frac{\ln(s_4/m^2)}{s_4}\right]_+ + c_{2\,gg}^{\rm 1PI}\left[\frac{1}{s_4}\right]_+ + c_{1\,gg}^{\rm 1PI}\delta(s_4)\right\}$$
$$+ \frac{\alpha_s^3(\mu_R^2)}{\pi}\left[A_{gg}^c\left[\frac{1}{s_4}\right]_+ + T_{1\,gg}^{c\,\rm 1PI}\,\delta(s_4)\right] . \qquad (3.1)$$

The Born term is given by

$$F_{gg}^{B\,\rm 1PI} = 2\pi\alpha_s^2(\mu_R^2)K_{gg}N_cC_F\left[C_F - C_A\frac{t_1u_1}{s^2}\right]B_{\rm QED} , \qquad (3.2)$$

where $K_{gg} = (N_c^2-1)^{-2}$ is a color average factor and

$$B_{\rm QED} = \frac{t_1}{u_1} + \frac{u_1}{t_1} + \frac{4m^2s}{t_1u_1}\left(1 - \frac{m^2s}{t_1u_1}\right) . \qquad (3.3)$$

We also define $c_{3\,gg}^{\rm 1PI} = 4C_A$,

$$c_{2\,gg}^{\rm 1PI} = -2C_A - 2C_A\ln\left(\frac{t_1u_1}{m^4}\right) - 2C_A\ln\left(\frac{\mu_F^2}{s}\right) \equiv T_{2\,gg}^{\rm 1PI} - 2C_A\ln\left(\frac{\mu_F^2}{s}\right) , \qquad (3.4)$$

$$c_{1\,gg}^{\rm 1PI} = \left[C_A\ln\left(\frac{t_1u_1}{m^4}\right) - \frac{\beta_0}{2}\right]\ln\left(\frac{\mu_F^2}{s}\right) + \frac{\beta_0}{2}\ln\left(\frac{\mu_R^2}{s}\right) , \qquad (3.5)$$

and

$$A_{gg}^c = \pi K_{gg}B_{\rm QED}(N_c^2-1)\left\{N_c\left(1 - \frac{2t_1u_1}{s^2}\right)\left[\left(-C_F + \frac{C_A}{2}\right)({\rm Re}L_\beta + 1) + \frac{N_c}{2} + \frac{N_c}{2}\ln\left(\frac{t_1u_1}{m^2s}\right)\right]\right.$$
$$\left. + \frac{1}{N_c}(C_F - C_A)({\rm Re}L_\beta + 1) - \ln\left(\frac{t_1u_1}{m^2s}\right) + \frac{N_c^2}{2}\frac{(t_1^2-u_1^2)}{s^2}\ln\left(\frac{u_1}{t_1}\right)\right\} . \qquad (3.6)$$

Finally,

$$T^{c\,1\mathrm{PI}}_{1\;gg} = \frac{\sigma^{(1)\,\mathrm{S+V}\,1\mathrm{PI}}_{gg\,\delta}}{\alpha_s^3/\pi} \tag{3.7}$$

where here $\sigma^{(1)\,\mathrm{S+V}\,1\mathrm{PI}}_{gg\,\delta}$ denotes the scale-independent $\delta(s_4)$ terms in the NLO cross section. These terms are given by Eq. (6.19) in Ref. [11].

The NNLO soft-plus-virtual corrections in 1PI kinematics are

$$\begin{aligned}
s^2\,\frac{d^2\hat{\sigma}^{(2)\,1\mathrm{PI}}_{gg}}{dt_1\,du_1} &= F^{B\,1\mathrm{PI}}_{gg}\frac{\alpha_s^2(\mu_R^2)}{\pi^2}\left\{\frac{1}{2}\left(c^{1\mathrm{PI}}_{3\;gg}\right)^2\left[\frac{\ln^3(s_4/m^2)}{s_4}\right]_+ + \left[\frac{3}{2}c^{1\mathrm{PI}}_{3\;gg}\,c^{1\mathrm{PI}}_{2\;q\overline{q}} - \frac{\beta_0}{4}c^{1\mathrm{PI}}_{3\;gg}\right]\left[\frac{\ln^2(s_4/m^2)}{s_4}\right]_+\right.\\
&+ \left[c^{1\mathrm{PI}}_{3\;gg}\,c^{1\mathrm{PI}}_{1\;gg} + \left(c^{1\mathrm{PI}}_{2\;gg}\right)^2 - \zeta_2\left(c^{1\mathrm{PI}}_{3\;gg}\right)^2 - \frac{\beta_0}{2}T^{1\mathrm{PI}}_{2\;gg} + \frac{\beta_0}{4}c^{1\mathrm{PI}}_{3\;gg}\ln\left(\frac{\mu_R^2}{s}\right) + 2C_AK\right]\left[\frac{\ln(s_4/m^2)}{s_4}\right]_+\\
&+ \left[c^{1\mathrm{PI}}_{2\;gg}\,c^{1\mathrm{PI}}_{1\;gg} - \zeta_2\,c^{1\mathrm{PI}}_{2\;gg}\,c^{1\mathrm{PI}}_{3\;gg} + \zeta_3\left(c^{1\mathrm{PI}}_{3\;gg}\right)^2 + \frac{\beta_0}{4}c^{1\mathrm{PI}}_{2\;gg}\ln\left(\frac{\mu_R^2}{s}\right) + \mathcal{G}^{(2)}_{gg}\right.\\
&\qquad + C_A\frac{\beta_0}{4}\ln^2\left(\frac{\mu_F^2}{s}\right) - C_AK\ln\left(\frac{\mu_F^2}{s}\right) - C_AK\ln\left(\frac{t_1u_1}{m^4}\right)\Big]\left[\frac{1}{s_4}\right]_+\\
&\left.+ R^{1\mathrm{PI}}_{gg}\delta(s_4)\right\}\\
&+ \frac{\alpha_s^4(\mu_R^2)}{\pi^2}\left\{\frac{3}{2}c^{1\mathrm{PI}}_{3\;gg}\,A^c_{gg}\left[\frac{\ln^2(s_4/m^2)}{s_4}\right]_+ + \left[\left(2\,c^{1\mathrm{PI}}_{2\;gg} - \frac{\beta_0}{2}\right)A^c_{gg} + c^{1\mathrm{PI}}_{3\;gg}T^{c\,1\mathrm{PI}}_{1\;gg} + F^c_{gg}\right]\left[\frac{\ln(s_4/m^2)}{s_4}\right]_+\right.\\
&+ \left[\left(c^{1\mathrm{PI}}_{1\;gg} - \zeta_2c^{1\mathrm{PI}}_{3\;gg} + \frac{\beta_0}{4}\ln\left(\frac{\mu_R^2}{s}\right)\right)A^c_{gg} + \left(c^{1\mathrm{PI}}_{2\;gg} - \frac{\beta_0}{2}\right)T^{c\,1\mathrm{PI}}_{1\;gg} + F^c_{gg}\,\ln\left(\frac{m^2}{s}\right)\right]\left[\frac{1}{s_4}\right]_+\\
&\left.+ R^{c\,1\mathrm{PI}}_{gg}\delta(s_4)\right\}\,,
\end{aligned} \tag{3.8}$$

where

$$\begin{aligned}
F^c_{gg} &= \frac{\pi}{2}K_{gg}B_{\mathrm{QED}}(N_c^2-1)\left\{2\ln\left(\frac{u_1}{t_1}\right)\frac{(t_1^2-u_1^2)}{s^2}\left[4\,\Gamma^{gg}_{11} + 2(N_c^2-2)\Gamma^{gg}_{22}\right]\right.\\
&+ \left(1 - \frac{2t_1u_1}{s^2}\right)N_c\left[4(\Gamma^{gg}_{22})^2 + (N_c^2+4)\ln^2\left(\frac{u_1}{t_1}\right)\right]\\
&\left.+ \frac{4}{N_c}\left[(\Gamma^{gg}_{11})^2 - 2(\Gamma^{gg}_{22})^2\right] - 2N_c\ln^2\left(\frac{u_1}{t_1}\right)\right\}\,,
\end{aligned} \tag{3.9}$$

with

$$\begin{aligned}
\Gamma^{gg}_{11} &\equiv -C_F\left(L'_\beta + 1\right) + C_A\,,\\
\Gamma^{gg}_{22} &\equiv -C_F\left(L'_\beta + 1\right) + \frac{C_A}{2}\left[2 + \ln\left(\frac{t_1u_1}{m^2s}\right) + L'_\beta\right]\,.
\end{aligned} \tag{3.10}$$

Here

$$\mathcal{G}^{(2)}_{gg} = C_A^2\left(\frac{7}{2}\zeta_3 + \frac{22}{3}\zeta_2 - \frac{41}{108}\right) + n_fC_A\left(-\frac{4}{3}\zeta_2 - \frac{5}{54}\right) \tag{3.11}$$

denotes a set of universal two-loop contributions for processes with gg initial states [8]; process-dependent two-loop corrections [10] are not included in $\mathcal{G}^{(2)}_{gg}$.

The contributions $R_{gg}^{1\mathrm{PI}}$ and $R_{gg}^{c\,1\mathrm{PI}}$ are virtual corrections that are not fully known. As in the $q\overline{q}$ channel, we keep only certain terms that can be determined exactly. The terms multiplying $\delta(s_4)$ involving the factorization and renormalization scales are

$$
\begin{aligned}
F_{gg}^{B\,1\mathrm{PI}}\frac{\alpha_s^2(\mu_R^2)}{\pi^2}\Bigg[&\ln^2\left(\frac{\mu_F^2}{m^2}\right)\left\{\frac{C_A^2}{2}\ln^2\left(\frac{t_1\,u_1}{m^4}\right)-\frac{5\beta_0}{8}C_A\ln\left(\frac{t_1\,u_1}{m^4}\right)+\frac{3\beta_0^2}{16}-2\zeta_2C_A^2\right\}\\
&+\ln\left(\frac{\mu_F^2}{m^2}\right)\ln\left(\frac{\mu_R^2}{m^2}\right)\frac{3\beta_0}{4}\left[C_A\ln\left(\frac{t_1\,u_1}{m^4}\right)-\frac{\beta_0}{2}\right]+\ln^2\left(\frac{\mu_R^2}{m^2}\right)\frac{3\beta_0^2}{16}\\
&+\ln\left(\frac{\mu_F^2}{m^2}\right)\Bigg\{C_A^2\ln^2\left(\frac{t_1\,u_1}{m^4}\right)\ln\left(\frac{m^2}{s}\right)-\frac{\beta_0}{2}C_A\ln\left(\frac{t_1\,u_1}{m^4}\right)\ln\left(\frac{m^2}{s}\right)\\
&\qquad+2C_A\zeta_2\left[T_{2\,gg}^{1\mathrm{PI}}-2C_A\ln\left(\frac{m^2}{s}\right)\right]-8C_A^2\zeta_3+C_A\frac{K}{2}\ln\left(\frac{t_1\,u_1}{m^4}\right)-2\gamma'^{(2)}_{g/g}\Bigg\}\\
&+\ln\left(\frac{\mu_R^2}{m^2}\right)\left\{\frac{3\beta_0}{4}C_A\ln\left(\frac{t_1\,u_1}{m^4}\right)\ln\left(\frac{m^2}{s}\right)+\frac{\beta_1}{8}\right\}\Bigg]\\
+\frac{\alpha_s^4(\mu_R^2)}{\pi^2}&\left\{\left[2C_A\zeta_2A_{gg}^c+\left(C_A\ln\left(\frac{t_1\,u_1}{m^4}\right)-\frac{\beta_0}{2}\right)T_{1\,gg}^{c\,1\mathrm{PI}}\right]\ln\left(\frac{\mu_F^2}{m^2}\right)+\frac{3\beta_0}{4}T_{1\,gg}^{c\,1\mathrm{PI}}\ln\left(\frac{\mu_R^2}{m^2}\right)\right\}
\end{aligned}
\tag{3.12}
$$

where

$$
\gamma'^{(2)}_{g/g}=C_A^2\left(\frac{2}{3}+\frac{3}{4}\zeta_3\right)-n_f\left(\frac{C_F}{8}+\frac{C_A}{6}\right)\,. \tag{3.13}
$$

The terms multiplying $\delta(s_4)$ that arise from inversion and do not involve the factorization and renormalization scales are

$$
\begin{aligned}
F_{gg}^{B\,1\mathrm{PI}}\frac{\alpha_s^2(\mu_R^2)}{\pi^2}&\left\{-\frac{\zeta_2}{2}\left[T_{2\,gg}^{1\mathrm{PI}}-2C_A\ln\left(\frac{m^2}{s}\right)\right]^2+\frac{1}{4}\zeta_2^2\left(c_{3\,gg}^{1\mathrm{PI}}\right)^2\right.\\
&\qquad\left.+\zeta_3\,c_{3\,gg}^{1\mathrm{PI}}\left[T_{2\,gg}^{1\mathrm{PI}}-2C_A\ln\left(\frac{m^2}{s}\right)\right]-\frac{3}{4}\zeta_4\left(c_{3\,gg}^{1\mathrm{PI}}\right)^2\right\}\\
+\frac{\alpha_s^4(\mu_R^2)}{\pi^2}&\left\{\left[\zeta_3c_{3\,gg}^{1\mathrm{PI}}-\zeta_2\left(T_{2\,gg}^{1\mathrm{PI}}-2C_A\ln\left(\frac{m^2}{s}\right)\right)\right]A_{gg}^c-\frac{\zeta_2}{2}F_{gg}^c\right\}\,.
\end{aligned}
\tag{3.14}
$$

3.2 $gg\to t\bar{t}$ channel in PIM kinematics

We continue our study of subleading terms in the gg channel by writing the $\overline{\mathrm{MS}}$ NLO soft-plus-virtual corrections for $gg\to t\bar{t}$ in PIM kinematics as

$$
\begin{aligned}
s\,\frac{d^2\hat{\sigma}_{gg}^{(1)\,\mathrm{PIM}}}{dM^2\,d\cos\theta}\;=\;&F_{gg}^{B\,\mathrm{PIM}}\frac{\alpha_s(\mu_R^2)}{\pi}\left\{c_{3\,gg}^{\mathrm{PIM}}\left[\frac{\ln(1-z)}{1-z}\right]_+\!+c_{2\,gg}^{\mathrm{PIM}}\left[\frac{1}{1-z}\right]_+\!+c_{1\,gg}^{\mathrm{PIM}}\delta(1-z)\right\}\\
&+\frac{\alpha_s^3(\mu_R^2)}{\pi}\left[A_{gg}^c\left[\frac{1}{1-z}\right]_+\!+T_{1\,gg}^{c\,\mathrm{PIM}}\,\delta(1-z)\right]\,.
\end{aligned}
\tag{3.15}
$$

Here the Born term is

$$
F_{gg}^{B\,\mathrm{PIM}}=\frac{\beta}{2s}F_{gg}^{B\,1\mathrm{PI}}|_{\mathrm{PIM}}\,. \tag{3.16}
$$

In addition, $c_{3\,gg}^{\mathrm{PIM}}=4C_A$,

$$
c_{2\,gg}^{\mathrm{PIM}}=-2C_A-2C_A\ln\left(\frac{\mu_F^2}{s}\right)\equiv T_{2\,gg}^{\mathrm{PIM}}-2C_A\ln\left(\frac{\mu_F^2}{s}\right)\,, \tag{3.17}
$$

$$c_{1\,gg}^{\rm PIM} = -\frac{\beta_0}{2}\ln\left(\frac{\mu_F^2}{s}\right) + \frac{\beta_0}{2}\ln\left(\frac{\mu_R^2}{s}\right) . \tag{3.18}$$

Finally,

$$T_{1\,gg}^{\rm PIM} = 2T_{1\,gg}^{\rm 1PI}|_{\rm PIM} + \frac{1}{\alpha_s^2} s\,\frac{d^2\sigma'^{(1)\ \rm S+MF}_{gg}}{dM^2\,d\cos\theta} - \frac{1}{\alpha_s^2}\frac{\beta}{s}\,s^2\,\frac{d^2\sigma'^{(1)\ \rm S+MF}_{gg}}{dt_1\,du_1}|_{\rm PIM} . \tag{3.19}$$

Here $\sigma'^{(1)\ \rm S+MF}_{gg}$ denotes the soft and mass factorization subtraction terms calculated in Ref. [3]. The prime indicates that we drop the overall $\delta(1-z)$ or $\delta(s_4)$ coefficients from the expressions in Eqs. (82), (A10), and (A11) of Ref. [3].

The NNLO soft-plus-virtual corrections in PIM kinematics are

$$\begin{aligned}
s\,\frac{d^2\hat\sigma_{gg}^{(2)\ \rm PIM}}{dM^2\,d\cos\theta} &= F_{gg}^{B\ \rm PIM}\frac{\alpha_s^2(\mu_R^2)}{\pi^2}\left\{\frac{1}{2}\left(c_{3\,gg}^{\rm PIM}\right)^2\left[\frac{\ln^3(1-z)}{1-z}\right]_+ + \left[\frac{3}{2}c_{3\,gg}^{\rm PIM}\,c_{2\,q\overline{q}}^{\rm PIM} - \frac{\beta_0}{4}c_{3\,gg}^{\rm PIM}\right]\left[\frac{\ln^2(1-z)}{1-z}\right]_+\right.\\
&+ \left[c_{3\,gg}^{\rm PIM}\,c_{1\,gg}^{\rm PIM} + \left(c_{2\,gg}^{\rm PIM}\right)^2 - \zeta_2\left(c_{3\,gg}^{\rm PIM}\right)^2 - \frac{\beta_0}{2}T_{2\,gg}^{\rm PIM} + \frac{\beta_0}{4}c_{3\,gg}^{\rm PIM}\ln\left(\frac{\mu_R^2}{s}\right) + 2C_AK\right]\left[\frac{\ln(1-z)}{1-z}\right]_+\\
&+ \left[c_{2\,gg}^{\rm PIM}\,c_{1\,gg}^{\rm PIM} - \zeta_2\,c_{2\,gg}^{\rm PIM}\,c_{3\,gg}^{\rm PIM} + \zeta_3\left(c_{3\,gg}^{\rm PIM}\right)^2 + \frac{\beta_0}{4}c_{2\,gg}^{\rm PIM}\ln\left(\frac{\mu_R^2}{s}\right) + \mathcal{G}_{gg}^{(2)}\right.\\
&\quad \left. + C_A\frac{\beta_0}{4}\ln^2\left(\frac{\mu_F^2}{s}\right) - C_AK\ln\left(\frac{\mu_F^2}{s}\right)\right]\left[\frac{1}{1-z}\right]_+\\
&\left. + R_{gg}^{\rm PIM}\delta(1-z)\right\}\\
&+ \frac{\alpha_s^4(\mu_R^2)}{\pi^2}\left\{\frac{3}{2}c_{3\,gg}^{\rm PIM}\,A'^c_{gg}\left[\frac{\ln^2(1-z)}{1-z}\right]_+ + \left[\left(2\,c_{2\,gg}^{\rm PIM} - \frac{\beta_0}{2}\right)A'^c_{gg} + c_{3\,gg}^{\rm PIM}T_{1\,gg}^{c\,\rm PIM} + F'^c_{gg}\right]\left[\frac{\ln(1-z)}{1-z}\right]_+\right.\\
&+ \left[\left(c_{1\,gg}^{\rm PIM} - \zeta_2 c_{3\,gg}^{\rm PIM} + \frac{\beta_0}{4}\ln\left(\frac{\mu_R^2}{s}\right)\right)A'^c_{gg} + \left(c_{2\,gg}^{\rm PIM} - \frac{\beta_0}{2}\right)T_{1\,gg}^{c\,\rm PIM}\right]\left[\frac{1}{1-z}\right]_+\\
&\left. + R_{gg}^{c\,\rm PIM}\delta(1-z)\right\} ,
\end{aligned} \tag{3.20}$$

with

$$A'^c_{gg} = \frac{\beta}{2s}A^c_{gg} , \qquad F'^c_{gg} = \frac{\beta}{2s}F^c_{gg} , \tag{3.21}$$

where A^c_{gg} and F^c_{gg} are the 1PI functions given in the previous subsection.

The virtual corrections $R_{gg}^{\rm PIM}$, $R_{gg}^{c\,\rm PIM}$ are also not fully known. We keep only certain terms that are determined exactly. The terms multiplying $\delta(1-z)$ that involve the factorization and renormalization scales are

$$\begin{aligned}
&F_{gg}^{B\ \rm PIM}\frac{\alpha_s^2(\mu_R^2)}{\pi^2}\left[\ln^2\left(\frac{\mu_F^2}{m^2}\right)\left\{\frac{3\beta_0^2}{16} - 2\zeta_2C_A^2\right\} - \frac{3\beta_0^2}{8}\ln\left(\frac{\mu_F^2}{m^2}\right)\ln\left(\frac{\mu_R^2}{m^2}\right) + \frac{3\beta_0^2}{16}\ln^2\left(\frac{\mu_R^2}{m^2}\right)\right.\\
&\qquad \left. + \ln\left(\frac{\mu_F^2}{m^2}\right)\left\{2C_A\zeta_2\left[T_{2\,gg}^{\rm PIM} - 2C_A\ln\left(\frac{m^2}{s}\right)\right] - 8C_A^2\zeta_3 - 2\gamma'^{(2)}_{g/g}\right\} + \frac{\beta_1}{8}\ln\left(\frac{\mu_R^2}{m^2}\right)\right]\\
&+ \frac{\alpha_s^4(\mu_R^2)}{\pi^2}\left\{\left[2C_A\zeta_2A'^c_{gg} - \frac{\beta_0}{2}T_{1\,gg}^{c\,\rm PIM}\right]\ln\left(\frac{\mu_F^2}{m^2}\right) + \frac{3\beta_0}{4}T_{1\,gg}^{c\,\rm PIM}\ln\left(\frac{\mu_R^2}{m^2}\right)\right\} .
\end{aligned} \tag{3.22}$$

The terms multiplying $\delta(1-z)$ that arise from inversion and do not involve the factorization and renormalization scales are

$$F_{gg}^{B\ \rm PIM}\frac{\alpha_s^2(\mu_R^2)}{\pi^2}\left\{-\frac{\zeta_2}{2}\left[T_{2\,gg}^{\rm PIM} - 2C_A\ln\left(\frac{m^2}{s}\right)\right]^2 + \frac{1}{4}\zeta_2^2\left(c_{3\,gg}^{\rm PIM}\right)^2\right.$$

$$+\zeta_3\, c_{3\,gg}^{\rm PIM}\left[T_{2\,gg}^{\rm PIM}-2C_A\ln\left(\frac{m^2}{s}\right)\right]-\frac{3}{4}\zeta_4\,\left(c_{3\,gg}^{\rm PIM}\right)^2\Bigg\}$$
$$+\frac{\alpha_s^4(\mu_R^2)}{\pi^2}\left\{\left[\zeta_3 c_{3\,gg}^{\rm PIM}-\zeta_2\left(T_{2\,gg}^{\rm PIM}-2C_A\ln\left(\frac{m^2}{s}\right)\right)\right]A'^c_{gg}-\frac{\zeta_2}{2}F'^c_{gg}\right\}. \tag{3.23}$$

4 Partonic cross sections

Any difference in the integrated cross sections due to kinematics choice arises from uncalculated subleading terms. At leading order (LO) the partonic threshold condition is exact and there is no difference between the total cross sections in the two kinematic schemes. However, beyond LO additional soft partons are produced and there is a difference when not all terms are known. The total partonic cross section may be expressed in terms of dimensionless scaling functions $f_{ij}^{(k,l)}$ that depend only on $\eta = s/4m^2 - 1$ [3],

$$\sigma_{ij}(s,m^2,\mu^2)=\frac{\alpha_s^2(\mu)}{m^2}\sum_{k=0}^{\infty}\,(4\pi\alpha_s(\mu))^k\sum_{l=0}^{k}\,f_{ij}^{(k,l)}(\eta)\,\ln^l\left(\frac{\mu^2}{m^2}\right). \tag{4.1}$$

These scaling functions all multiply powers of $\ln(\mu^2/m^2)$ and thus do not depend on μ themselves. Here we have set $\mu \equiv \mu_F = \mu_R$. We work in the $\overline{\rm MS}$ scheme throughout.

Previously, we constructed LL, NLL, and NNLL approximations to $f_{ij}^{(k,l)}$ in the $q\overline{q}$ and gg channels for $k \le 2$, $l \le k$ [3]. We now present the full soft-plus-virtual results for the $f_{ij}^{(2,1)}$ and $f_{ij}^{(2,2)}$ scaling functions and the partial results for $f_{ij}^{(2,0)}$ that include the soft NNNLL and those virtual terms calculated in sections 2 and 3.

We begin with a comparison of the full soft-plus-virtual 1PI and PIM contributions to $f_{ij}^{(2,1)}$ and $f_{ij}^{(2,2)}$, shown in Fig. 1. The upper plots are for the $q\overline{q}$ channel. The left-hand side of Fig. 1 compares the 1PI and PIM scaling functions for $f_{q\overline{q}}^{(2,1)}$. At low η, closer to partonic threshold, the agreement is very good, better than that obtained at NNLL in Ref. [3]. The agreement is also improved at large η. The right-hand side shows the $f_{q\overline{q}}^{(2,2)}$ scaling functions in both kinematics. The results for $f_{q\overline{q}}^{(2,2)}$ remain unchanged from those of Ref. [3]. The agreement between the two kinematics choices is excellent.

The lower plots of Fig. 1 show the corresponding scaling functions in the gg channel. The agreement between the two kinematics choices is somewhat improved at high η as compared to previous NNLL results [3]. We note that there is some ambiguity in the way that the expressions for the gg partonic cross sections can be written at threshold. We have investigated the effect of replacing $1 - 2t_1u_1/s^2$ with $(t_1^2+u_1^2)/s^2$ in Eq. (3.6), more consistent with the expressions in Ref. [11]. These two expressions are equivalent at threshold, $s_4 = 0$ and $z = 1$, but can differ at large η. Note that $f_{gg}^{(2,2)}$ is not affected by this replacement. The resulting differences in $f_{gg}^{(2,1)}$ are small, appearing only at $\eta > 0.1$ where the agreement between the scaling functions in the two kinematics begins to diverge. The main effect of the second choice is to make the PIM result for $f_{gg}^{(2,1)}$ more negative at large η. We thus use the expressions as written in the text to be consistent with those of Ref. [3].

We now turn to the $f_{ij}^{(2,0)}$ scaling functions, the most important contributions at NNLO and independent of $\ln(\mu^2/m^2)$. We add the NNNLL terms, i.e. terms proportional to $[1/s_4]_+$ (1PI) and $[1/(1-z)]_+$ (PIM), to our previous NNLO-NNLL calculation. We also investigate the

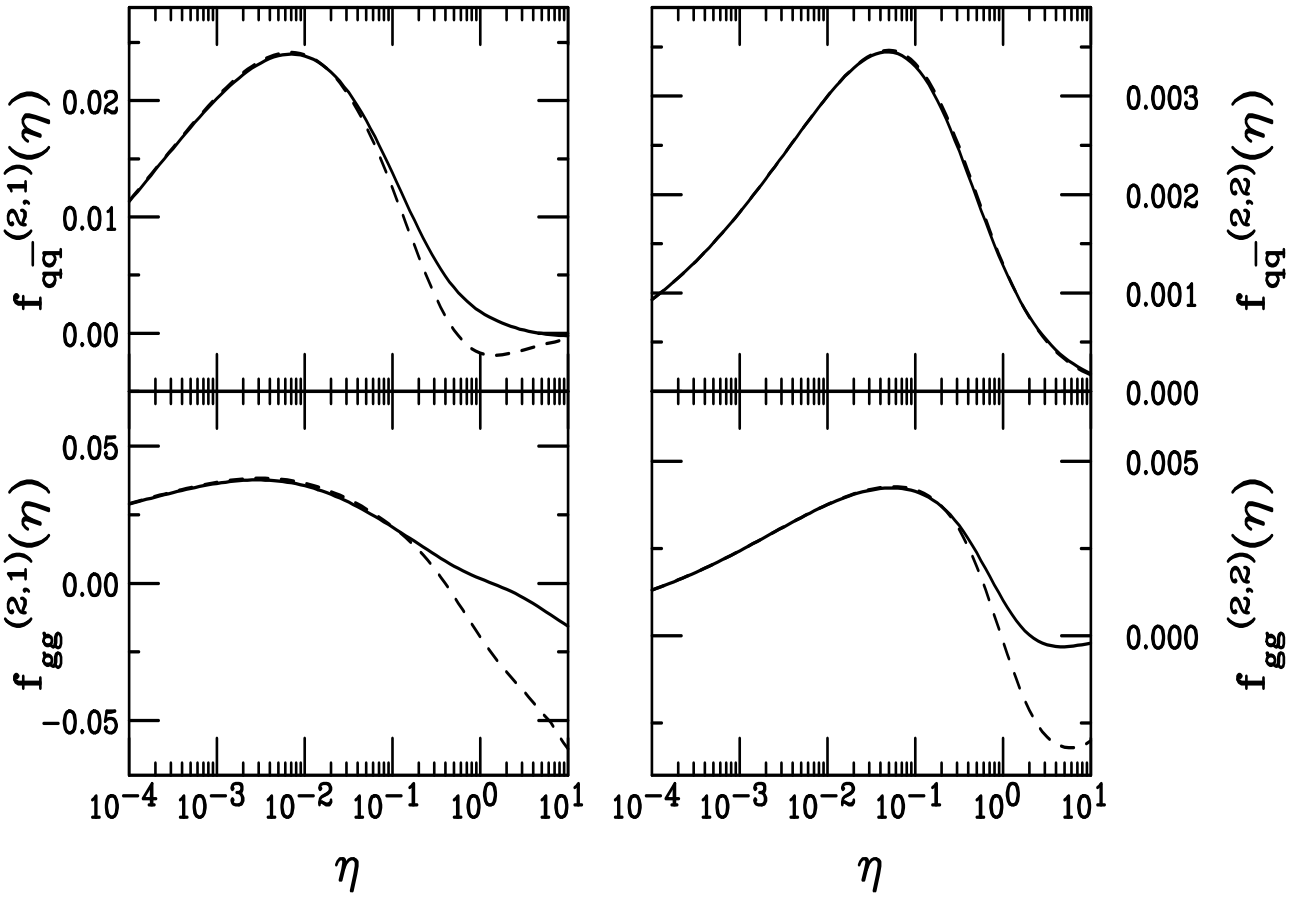

Figure 1: The $\overline{\rm MS}$ scheme scaling functions multiplying the scale-dependent logarithms, $f_{ij}^{(2,1)}$ (left-hand side) and $f_{ij}^{(2,2)}$ (right-hand side). The upper plots are for the $q\overline{q}$ channel while the lower plots are for the gg channel. The solid curves are for 1PI kinematics, the dashed for PIM kinematics.

effect of keeping the virtual ζ terms resulting from the inversion from moment to momentum space. To demonstrate the effect of adding successive subleading contributions, in Fig. 2 we show the NNLL results in the upper plots, the scaling functions through NNNLL in the middle plots, and the results with the NNNLL and virtual ζ terms in the lower plots.

We first discuss the results for the $q\overline{q}$ channel in the $\overline{\rm MS}$ scheme, shown on the left-hand side of Fig. 2. Note that to NNLL, the two kinematics choices give rather different results, even at low η. When the NNNLL contribution is added, both the 1PI and PIM results are reduced relative to the NNLL over all η. The agreement between the two kinematics is much improved up to $\eta > 0.01$. Adding the virtual ζ terms resulting from inversion improves the agreement between the 1PI and PIM kinematics further for $0.01 < \eta < 0.1$. At $\eta > 0.1$, the region where the parton luminosity peaks for $t\overline{t}$ production at the Tevatron, the additional virtual ζ terms provide a further small reduction. With the subleading terms, the 1PI result is smaller than previously but positive while the PIM result becomes more negative. However, on the whole, the subleading terms bring the 1PI and PIM results into better agreement over all η. We note here that the effect of the virtual ζ terms is numerically small, as is also the case for the gg channel and for the hadronic results for both channels in the next section. This small effect is in

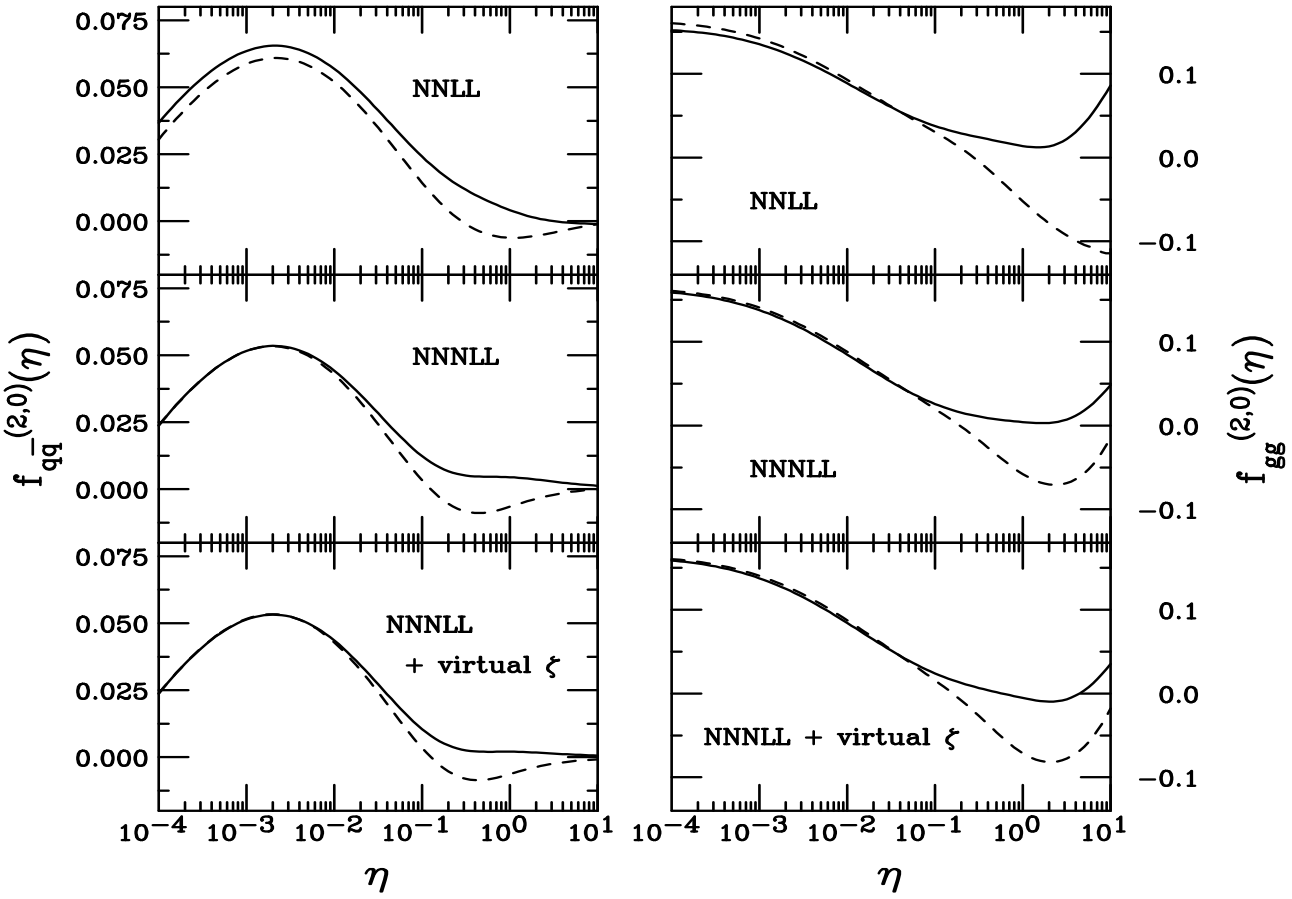

Figure 2: The $f_{ij}^{(2,0)}$ scaling functions in the $\overline{\rm MS}$ scheme. The left-hand side shows the results for the $q\overline{q}$ channel while the right-hand side shows the results for the gg channel. The top plots show the NNLL result from Ref. [3]. The center plots give the results through NNNLL and the bottom plots give the results including the virtual ζ terms. The solid curves are for 1PI kinematics, the dashed for PIM kinematics.

agreement with the arguments in Section IIIC of Ref. [2] concerning resummation prescriptions. There it was shown that when subleading terms from inversion are calculated exactly they do not have an unwarrantedly large effect on the numerical results.

A similar trend is seen for the gg channel on the right-hand side of Fig. 2. The agreement between the NNLL 1PI and PIM scaling functions at low η is significantly better than in the $q\overline{q}$ channel. This may perhaps be a consequence of the more complex color structure of the gg channel. Note however the significant divergence at large η. The 1PI NNLL result is large and positive while the PIM is large and negative. Again, inclusion of the subleading contributions improves agreement over all η. There is only a small improvement possible at low η. However, the improvement at larger η, $\eta > 0.1$ is notable. The 1PI result with soft NNNLL plus virtual ζ terms is reduced by nearly a factor of two relative to the NNLL result at $\eta = 10$. Likewise, the subleading terms stop and reverse the downward trend of the PIM scaling functions. The 1PI gg contribution will still be positive while the PIM will still be negative but the difference may not be as large as before. Using the alternate expression, $(t_1^2 + u_1^2)/s^2$, in Eq. (3.6) does not significantly change the results, particularly for 1PI kinematics. The PIM result becomes

slightly more negative at intermediate η, $\eta \approx 1$.

Finally we note that if we had kept only the ζ contributions in the $[1/s_4]_+$ and $[1/(1-z)]_+$ terms the 1PI and PIM results would not have agreed near threshold. The full NNNLL result, given in sections 2 and 3, is required for the result to be independent of kinematics choice near threshold. This agreement also indicates that additional two-loop contributions not included in our expressions should be small.

We now turn to our calculations of the hadronic total cross sections and transverse momentum distributions.

5 Hadronic total cross sections and p_T distributions

The inclusive hadronic cross section is obtained by convoluting the inclusive partonic cross sections with the parton luminosity, Φ_{ij}, defined as

$$\Phi_{ij}(\tau,\mu_F^2) \;=\; \tau \int_0^1 dx_1 \int_0^1 dx_2 \; \delta(x_1 x_2 - \tau) \; \phi_{i/h_1}(x_1,\mu_F^2)\, \phi_{j/h_2}(x_2,\mu_F^2)\,, \tag{5.1}$$

where $\phi_{i/h}(x,\mu_F^2)$ is the density of partons of flavor i in hadron h carrying a fraction x of the initial hadron momentum, at factorization scale μ_F. Then

$$\begin{aligned} \sigma_{h_1 h_2}(S,m^2) \;&=\; \sum_{i,j=q,\overline{q},g} \int_{4m^2/S}^1 \frac{d\tau}{\tau} \; \Phi_{ij}(\tau,\mu_F^2) \; \sigma_{ij}(\tau S, m^2, \mu_F^2) \\ &=\; \sum_{i,j=q,\overline{q},g} \int_{-\infty}^{\log_{10}(S/4m^2-1)} d\log_{10}\eta \, \frac{\eta}{1+\eta} \ln(10) \, \Phi_{ij}(\eta,\mu_F^2) \; \sigma_{ij}(\eta, m^2, \mu_F^2) \end{aligned} \tag{5.2}$$

where

$$\eta = \frac{s}{4m^2} - 1 \;=\; \frac{\tau S}{4m^2} - 1\,, \tag{5.3}$$

and S is the hadronic Mandelstam invariant. Our investigations in Ref. [3] showed that the approximation should hold if the convolution of the parton densities is not very sensitive to the high η region.

We use the recent MRST2002 NNLO (approximate) parton densities [12] with an NNLO evaluation of α_s. The parton luminosities, weighted to emphasize the most important contributions to the hadronic cross sections, are shown for $\sqrt{S} = 1.96$ TeV in Fig. 3. The $q\overline{q}$ luminosity is nearly 50% higher than the CTEQ5M [13] $q\overline{q}$ luminosity used in Ref. [3]. The gg luminosities for the two sets are rather similar. The peak of the luminosity is at $\eta < 1$, but still in a regime where the 1PI and PIM results differ most. Fortunately the gg luminosity is small compared to the $q\overline{q}$ luminosity since the differences in the kinematics is largest in the gg channel.

Our calculations use the exact LO and NLO cross sections with the soft NNNLL and virtual ζ corrections and the full soft-plus-virtual scale-dependent terms at NNLO. In addition we multiply the NNLO scaling functions by a damping factor, $1/\sqrt{1+\eta}$, as in Ref. [3], to lessen the influence of the large η region where the threshold approximation does not hold so well.

In Fig. 4, we present the NLO and approximate NNLO $t\bar{t}$ cross sections at $\sqrt{S} = 1.8$ TeV (left-hand side) and 1.96 TeV (right-hand side) as functions of top quark mass for $\mu = m$. The

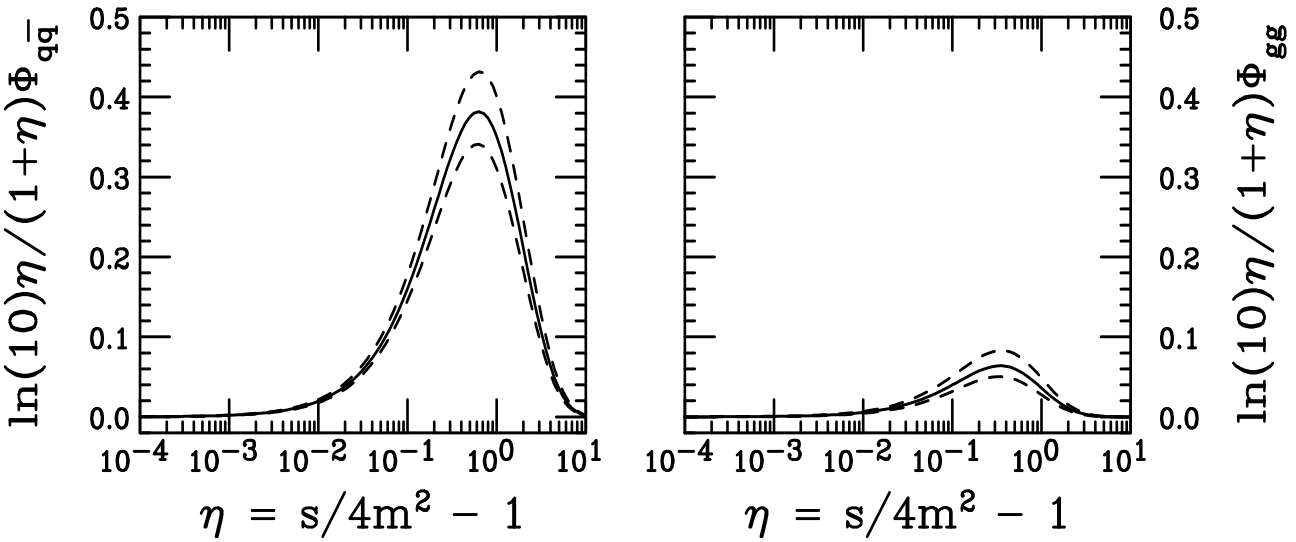

Figure 3: The $q\overline{q}$ (left-hand side) and gg (right-hand side) parton luminosities in $p\overline{p}$ collisions at $\sqrt{S} = 1.96$ TeV. The solid curves are calculated with $\mu = m = 175$ GeV while the upper dashed curves are with $\mu = m/2$ and the lower dashed curves with $\mu = 2m$.

NNLO results include the soft NNNLL and virtual ζ terms in 1PI and PIM kinematics. We also show the average of the two kinematics results which may perhaps be closer to the full NNLO result. Here the NNLO PIM cross section is slightly lower than the NLO cross section for all masses shown. In Ref. [3], the PIM cross section was a bit higher than the NLO. The reduction of the PIM $q\overline{q}$ result, dominant for $p\overline{p} \to t\overline{t}$, lowers the total PIM cross section. The NNLO 1PI cross section remains above the NLO for all m although the NNLO cross section is not as large as previously, due to the subleading terms. The average of the two kinematics is just above the NLO cross sections for both energies.

Going to higher scales increases all the NNLO corrections so that both kinematics choices give cross sections larger than the NLO. On the other hand, at lower scales, the NNLO cross sections are reduced relative to the NLO. The ratio of the NNLO to the NLO cross sections, the K factors, are shown in Fig. 5 as functions of mass for $\mu = m$ (upper plot), $2m$ (middle plot and $m/2$ (lower plot) at $\sqrt{S} = 1.8$ TeV. In keeping with the results in Fig. 4, for $\mu = m$ $K < 1$ for PIM kinematics, > 1 for 1PI and for the average. The K factors are larger for $\mu = 2m$ and smaller for $\mu = m/2$. Note also that K is almost independent of m. We remark that the NLO/LO K factor, while also essentially mass independent, is typically larger than the NNLO/NLO K factors shown here. It is ~ 1.25 for $\mu = m$, 1.52 for $\mu = 2m$ and 0.94 for $\mu = m/2$. Only the last value is similar to that of the NNLO/NLO average K factor in Fig. 5. The small K factors, obtained with results calculated with the MRST NNLO parton distribution functions at each order, indicate good convergence. Even though the results are shown at $\sqrt{S} = 1.8$ TeV, the K factors at $\sqrt{S} = 1.96$ TeV are very similar.

We now examine the scale dependence in Fig. 6 as a function of top quark mass and in Fig. 7 as a function of μ/m with $m = 175$ GeV. Figure 6 shows the ratio of the cross sections with $\mu = 2m$ to $\mu = m$ on the left-hand side and the ratio for $\mu = m/2$ to $\mu = m$ on the right-hand side at both NLO and NNLO at $\sqrt{S} = 1.8$ TeV. The ratios are nearly independent of mass at this energy. The scale dependence is reduced at NNLO relative to NLO. The NNLO results are very similar for the two ratios. In contrast, the LO scale dependence is much larger,

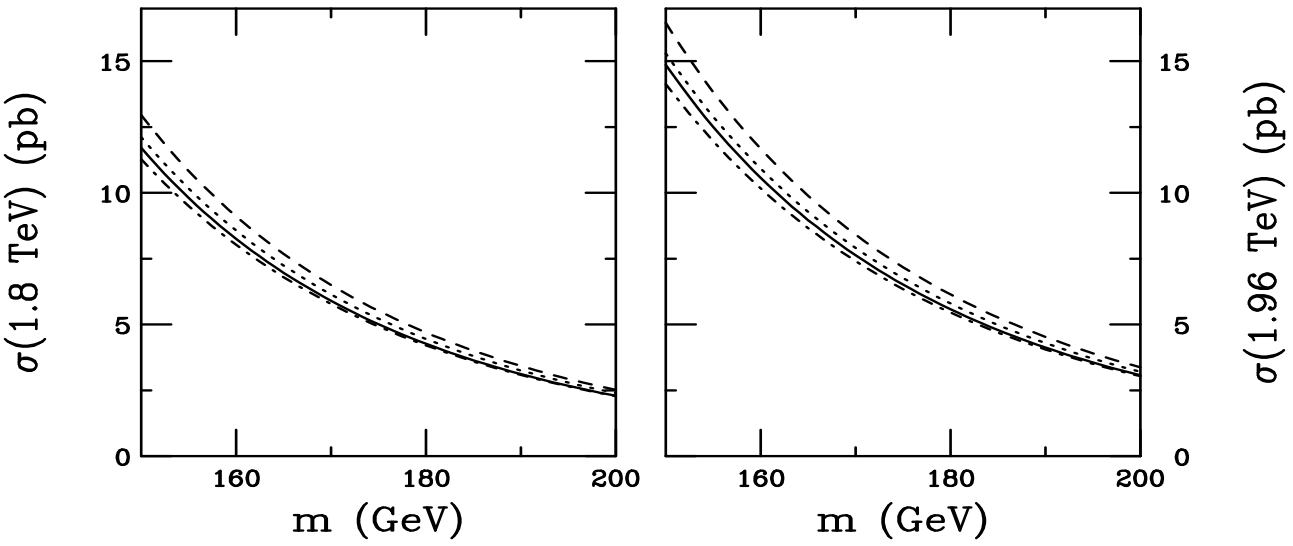

Figure 4: The $t\bar{t}$ total cross sections in $p\bar{p}$ collisions at $\sqrt{S} = 1.8$ TeV (left-hand side) and 1.96 TeV (right-hand side) as functions of m for $\mu = m$. The NLO (solid), and approximate NNLO 1PI (dashed), PIM (dot-dashed) and average (dotted) results are shown.

$\sigma(\mu = 2m)/\sigma(\mu = m) \approx 0.74$ and $\sigma(\mu = m/2)/\sigma(\mu = m) \approx 1.4$. The difference between the scale dependence at $\sqrt{S} = 1.8$ TeV and 1.96 TeV is negligible.

We have also calculated the cross sections as functions of μ/m for $0.2 < \mu/m < 10$ at $\sqrt{S} = 1.96$ TeV and $m = 175$ GeV in Fig. 7. The NLO cross section is not as strong a function of μ/m as the LO cross section. In fact, it is seen to rise with μ/m and then turn over. The NNLO cross sections, however, exhibit even less dependence on μ/m, approaching the independence of scale corresponding to a true physical cross section. They change by less than 15% over the entire range of μ/m considered. The change in the NNLO cross sections through the range $m/2 < \mu < 2m$, normally displayed as a measure of uncertainty from scale variation, is less than 3%. Note also that, at this energy, the absolute difference between the 1PI and PIM cross sections is also not large.

In Table 1, we give the NLO, NNLO 1PI and NNLO PIM $t\bar{t}$ total cross sections at $\sqrt{S} = 1.8$ and 1.96 TeV for $p\bar{p}$ interactions, corresponding to Tevatron Runs I and II. The results are presented for $m = 175$ GeV and $\mu = m/2$, m, and $2m$. We show the results of our calculations with the MRST2002 NNLO parton densities [12] and the three-loop α_s. We compare these with results of calculations with the CTEQ6M NLO parton densities [14] and the two-loop α_s. The results with the two different sets of parton densities are quite similar even though the parton densities are evaluated to different orders. Note that the NNLO scale dependence is negligible compared to the NLO scale dependence. The kinematics dependence of the NNLO cross sections thus remains the largest source of uncertainty. At $\sqrt{S} = 1.8$ TeV, averaging over the 1PI and PIM NNLO results with the two sets of parton distributions at $\mu = m = 175$ GeV, our best estimate for the cross section is 5.24 ± 0.31 pb where the quoted uncertainty is from the kinematics dependence. At $\sqrt{S} = 1.96$ TeV our corresponding best estimate is 6.77 ± 0.42 pb.

We note that the cross sections presented in Table 1 are significantly lower than our previous estimates [2, 3] at both NLO and NNLO. The difference at NLO is solely due to the new sets of parton densities used here, MRST2002 and CTEQ6M, relative to CTEQ5M in Refs. [2, 3]. Our

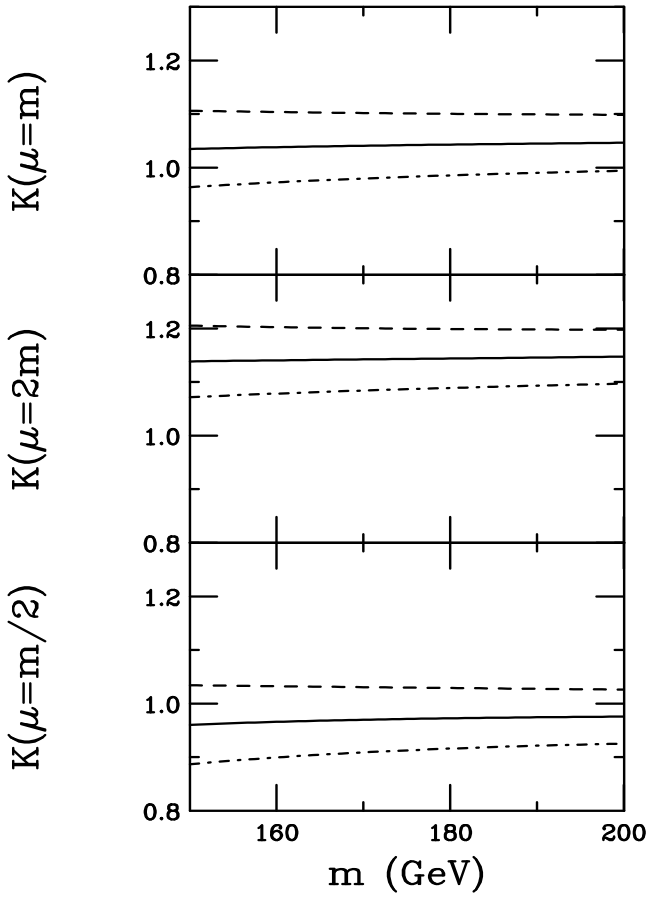

Figure 5: The NNLO K factors at $\sqrt{S} = 1.8$ TeV as functions of top quark mass in $p\overline{p}$ collisions with $\mu = m$ (upper), $\mu = 2m$ (middle) and $\mu = m/2$ (lower). The curves show the ratio of the approximate NNLO 1PI (dashed), PIM (dot-dashed) and average (solid) cross sections to the NLO cross section.

new NLO results are around 3% lower. The effect of the new densities on the NNLO corrections is even larger. The NNLO-NNLL 1PI corrections are smaller than our previous results [2, 3] by 14% for $\mu = m$ and 18% for $\mu = 2m$ with the MRST2002 NNLO densities. Most of this difference is in the relative values of α_s between the two sets. In addition, the new subleading terms we have included here further reduce the magnitude of the NNLO corrections. The combined effect of the new parton densities and new subleading terms make our new estimates for the total NNLO $t\overline{t}$ cross section noticeably smaller.

In Fig. 8 we show the top quark transverse momentum distributions at $\sqrt{S} = 1.8$ and 1.96 TeV. The NLO and NNLO 1PI results are shown using the MRST2002 NNLO densities. Details of the hadronic calculation of the p_T dependence are given in Appendix B of Ref. [2]. At NNLO we observe an enhancement of the NLO distribution with no significant change in shape. This pattern agrees with earlier resummed results on top transverse momentum and rapidity distributions [2, 15].

Finally we discuss top production in pp collisions at the LHC. The weighted parton luminosities are shown in Fig. 9 for the maximum LHC pp energy, $\sqrt{S} = 14$ TeV. The gg luminosity now dominates the $q\overline{q}$ by a factor of 4. The peak of the luminosity is still at $\eta \leq 1$ so that this energy is not very far from partonic threshold. However, large uncertainties may be expected

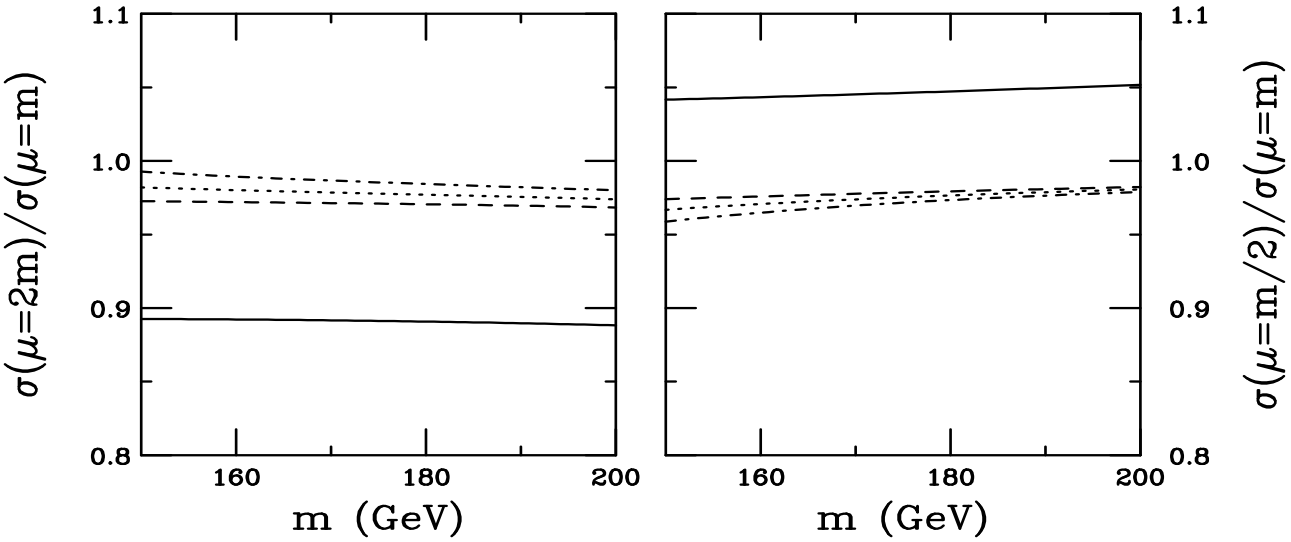

Figure 6: The scale dependence of the $t\bar{t}$ total cross sections in $p\overline{p}$ collisions at $\sqrt{S} = 1.8$ TeV as a function of top quark mass. The left-hand side shows the ratio $(\mu = 2m)/(\mu = m)$ while the right-hand side gives the ratio for $(\mu = m/2)/(\mu = m)$. The NLO (solid), and approximate NNLO 1PI (dashed), PIM (dot-dashed) and average (dotted) results are shown.

in the gg channel since the difference in the kinematics choice, largest in this channel, will be emphasized by the high gg luminosity.

Since the gg contribution dominates at high energy, the difference in the results for the two kinematics increases strongly with energy. The complex color structure of the gg channel may be better suited to 1PI kinematics and thus this kinematics choice could be more appropriate in processes where the gg channel dominates, see Ref. [7] for discussions of bottom and charm production. The NNLO 1PI scale dependence at high energy seems to support such a conclusion. At $\sqrt{S} = 14$ TeV, the NNLO 1PI scale dependence is 4%, smaller than the 9% dependence of the NLO cross section, an acceptable behavior, similar to that at the Tevatron. However, the NNLO gg PIM contribution is large and negative. The $q\overline{q}$ PIM contribution is also negative for $\mu \leq m$ albeit much smaller than the gg contribution. The NNLO PIM cross section is reduced by nearly a factor of two relative to the NLO. The scale dependence is similarly large. Thus we will only provide NNLO 1PI results for the LHC. At $\sqrt{S} = 14$ TeV with $m = 175$ GeV and the MRST2002 NNLO parton densities, the NLO cross section is 808.8 pb for $\mu = m/2$, 794.1 pb for $\mu = m$, and 744.4 pb for $\mu = 2m$. The corresponding NNLO 1PI cross sections are 845.2 pb for $\mu = m/2$, 872.8 pb for $\mu = m$, and 875.1 pb for $\mu = 2m$. In Fig. 10 we show the NLO and NNLO 1PI top quark p_T distributions at $\sqrt{S} = 14$ TeV. Here also the NNLO corrections enhance the NLO result without a change in shape.

6 Conclusions

In this paper we have calculated soft NNLO corrections to the total top quark cross section and top transverse momentum distributions in hadron-hadron collisions. We have added new soft NNNLL terms and some virtual terms, including all soft-plus-virtual factorization and renormalization scale terms. We have found that these new subleading corrections greatly diminish

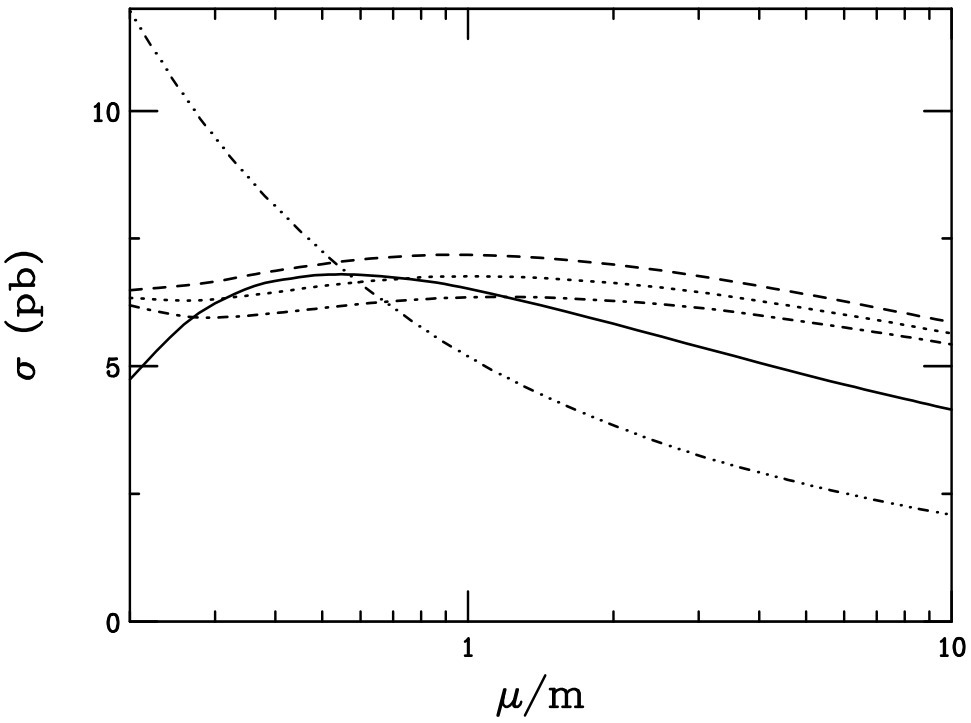

Figure 7: The scale dependence of the $t\bar{t}$ total cross sections in $p\overline{p}$ collisions at $\sqrt{S} = 1.96$ TeV as a function of μ/m. The LO (dot-dot-dot-dashed), NLO (solid), and approximate NNLO 1PI (dashed), PIM (dot-dashed) and average (dotted) results are shown.

the dependence of the cross section on the kinematics and on the factorization/renormalization scales. We have provided numerical results for the total cross section and top transverse momentum distributions for top quark production at the Tevatron, at both Run I and II, and at the LHC.

Acknowledgements

The research of N.K. has been supported by a Marie Curie Fellowship of the European Community programme "Improving Human Research Potential" under contract number HPMF-CT-2001-01221. The research of R.V. is supported in part by the Division of Nuclear Physics of the Office of High Energy and Nuclear Physics of the U.S. Department of Energy under Contract No. DE-AC-03-76SF00098.

References

[1] CDF Collaboration, F. Abe *et al.*, Phys. Rev. Lett. **74**, 2626 (1995);
D0 Collaboration, S. Abachi *et al.*, Phys. Rev. Lett. **74**, 2632 (1995).

[2] N. Kidonakis, Phys. Rev. D **64**, 014009 (2001).

[3] N. Kidonakis, E. Laenen, S. Moch, and R. Vogt, Phys. Rev. D **64**, 114001 (2001).

σ (pb)							
		MRST2002 NNLO			CTEQ6M		
$\sqrt{S}$ (TeV)	Order	$\mu = m/2$	$\mu = m$	$\mu = 2m$	$\mu = m/2$	$\mu = m$	$\mu = 2m$
	NLO	5.24	5.01	4.46	5.27	5.06	4.51
1.8	NNLO 1PI	5.40	5.52	5.36	5.43	5.58	5.43
	NNLO PIM	4.78	4.92	4.85	4.76	4.94	4.89
	NLO	6.79	6.52	5.83	6.79	6.54	5.85
1.96	NNLO 1PI	7.00	7.17	6.99	7.01	7.21	7.04
	NNLO PIM	6.14	6.35	6.28	6.08	6.33	6.29

Table 1: The $\overline{\rm MS}$ top quark production cross section in $p\overline{p}$ collisions at the Tevatron ($\sqrt{S} = 1.8$ and 1.96 TeV) for $m = 175$ GeV. The NLO results are exact while the approximate NNLO results include the soft NNNLL corrections and the virtual ζ terms as well as the full soft-plus-virtual scale dependence.

[4] N. Kidonakis and G. Sterman, Phys. Lett. B **387**, 867 (1996); Nucl. Phys. **B505**, 321 (1997).

[5] N. Kidonakis, G. Oderda, and G. Sterman, Nucl. Phys. **B525**, 299 (1998); **B531**, 365 (1998); N. Kidonakis, Int. J. Mod. Phys. A **15**, 1245 (2000).

[6] E. Laenen, G. Oderda, and G. Sterman, Phys. Lett. B **438**, 173 (1998).

[7] N. Kidonakis, E. Laenen, S. Moch, and R. Vogt, Phys. Rev. D **67**, 074037 (2003); Nucl. Phys. **A715**, 549c (2003).

[8] N. Kidonakis, hep-ph/0303186.

[9] W. Beenakker, W.L. van Neerven, R. Meng, G.A. Schuler, and J. Smith, Nucl. Phys. **B351**, 507 (1991).

[10] N. Kidonakis, hep-ph/0208056.

[11] W. Beenakker, H. Kuijf, W.L. van Neerven, and J. Smith, Phys. Rev. D **40**, 54 (1989).

[12] A.D. Martin, R.G. Roberts, W.J. Stirling, and R.S. Thorne, Eur. Phys. J. C **28**, 455 (2003).

[13] CTEQ Collaboration, H.L. Lai *et al.*, Eur. Phys. J. C **12**, 375 (2000).

[14] J. Pumplin, D.R. Stump, J. Huston, H.L. Lai, P. Nadolsky, and W.K. Tung, JHEP 0207, **012** (2002).

[15] N. Kidonakis and J. Smith, Phys. Rev. D **51**, 6092 (1995).

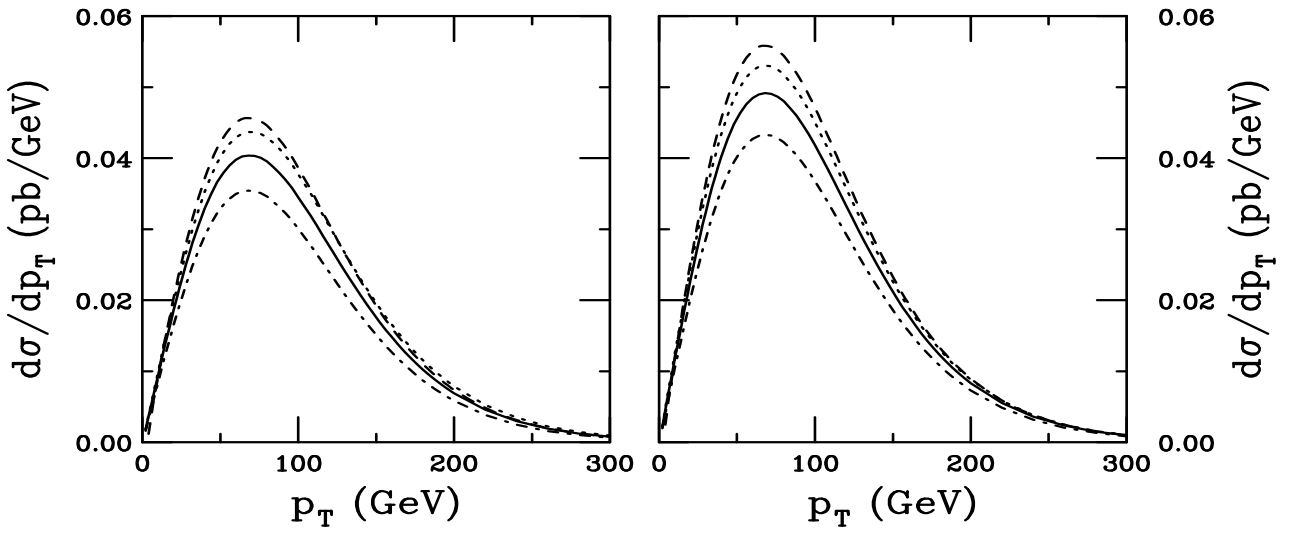

Figure 8: The top quark transverse momentum distribution with $m = 175$ GeV at $\sqrt{S} = 1.8$ TeV (left) and 1.96 TeV (right). The NLO (solid $\mu = m$, dotted $\mu = m/2$, dot-dashed $\mu = 2m$), and approximate NNLO ($\mu = m$) 1PI (dashed) results are shown.

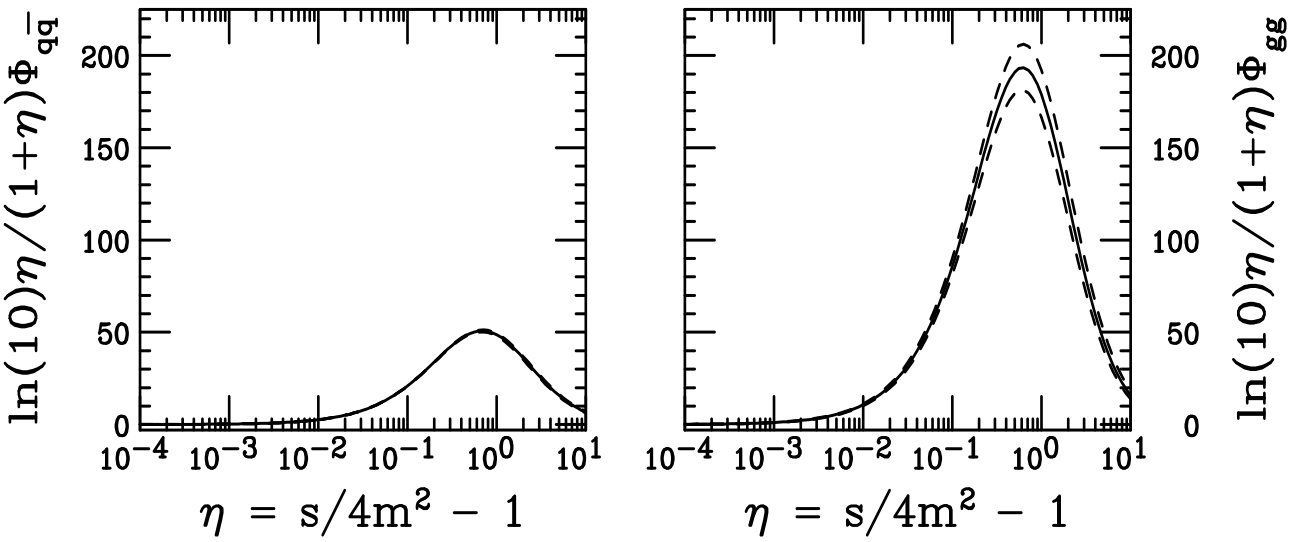

Figure 9: The $q\overline{q}$ (left-hand side) and gg (right-hand side) parton luminosities in pp collisions at $\sqrt{S} = 14$ TeV. The solid curves are calculated with $\mu = m = 175$ GeV while the upper dashed curves are with $\mu = m/2$ and the lower dashed curves with $\mu = 2m$.

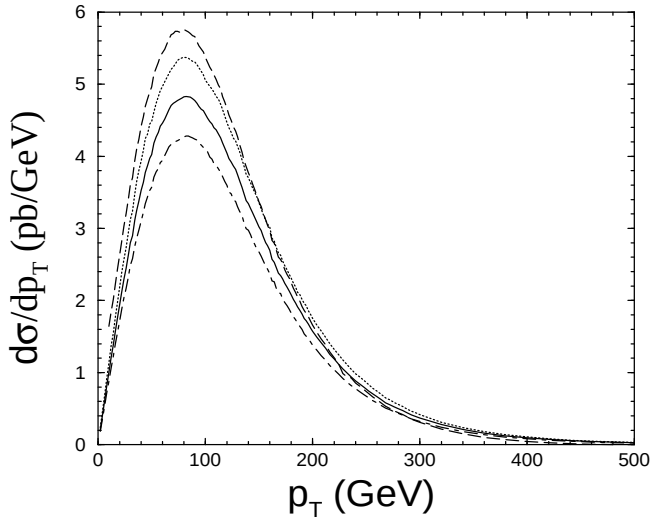

Figure 10: The top quark transverse momentum distribution with $m = 175$ GeV at $\sqrt{S} = 14$ TeV. The NLO (solid $\mu = m$, dotted $\mu = m/2$, dot-dashed $\mu = 2m$), and approximate NNLO ($\mu = m$) 1PI (dashed) results are shown.